ASTFE American Society of Thermal and Fluids Engineers

Proceedings of the 1st Thermal and Fluid Engineering Summer Conference, TFESC
August 9-12, 2015, New York City, USA

TFESC-13235

Mass Balance in Velocity Dirichlet Boundary Conditions for Lattice Boltzmann Method

Zheng Li[1,2], Mo Yang[1], Yaling He[3] and Yuwen Zhang[2,3*]

[1] University of Shanghai for Science and Technology, Shanghai 200093, China
[2] University of Missouri, Columbia, MO 65211, USA
[3] Xi'an Jiaotong University, Shaanxi 710049, China

ABSTRACT

Many different methods can be used to treat open boundary conditions in lattice Boltzmann method. Zou-He method, finite difference velocity gradient method, and regularized method are reviewed and compared for velocity Dirichlet condition for Poiseuille flow with different Reynolds numbers. Using same convergence criterion, all the numerical procedures are carried on till steady-states are reached. The obtained velocities and pressures are compared with analytical solutions and mass balances for different methods are also checked. The results indicates all the numerical results agree with analytical solutions well and Zou-He method results satisfy the mass balance better than the others.

KEY WORDS: Zou-He method, Finite difference velocity gradient method, Regularized method, Lattice Boltzmann method, Velocity Dirichlet condition

1. INTRODUCTION

Lattice Boltzmann method (LBM) [1] has developed to be a powerful numerical method for fluid flow simulation in last three decades. Traditional computational fluid dynamic (CFD) methods, such as finite volume method (FVM) and finite difference method (FDM), solve differenced mass and momentum equations to obtain the velocity, density, and pressure directly. Different from them, LBM solves mesoscopic parameter density distribution first And then use them to calculate the macroscopic parameters, which can also satisfy the mass and momentum equations. The LBM has been applied to many fluid flow and heat transfer problems, including incompressible fluid flow [2, 3], porous media fluid flow [4, 5] and phase change problems [6, 7]. Comparing with the traditional methods, LBM shows its advantages in easy code settings, applicability in parallel computing, and suitability to complex fluid flow. Several hybrid methods are developed to take advantages of both CFD and LBM [8, 9].

Some basic problems still remain in this algorithm. For example, there are many boundary condition setting methods in LBM without reaching an agreement. Latt and Chopard [10] compared five common boundary conditions in straight boundary and suggested that all those methods can reach the same accuracy macroscopic results for several cases. Collison and streaming are two basic processes in LBM. Its boundary conditions fall into two categories: (1) recovering the unknown density distribution step after streaming step on the boundary, (2) replacing all the density distributions. These methods show valid difference when the boundary speed is not zero. In that case, the density distributions entering the system are not equal to that leaving the system which violates local mass balance [11].

Numerous efforts have been made to study the cases of non-zero velocity to discuss local mass balance for the LBM boundary. A curved boundary treatment was proposed in Refs. [12, 13]. The no-slip curved boundary is approximated to be a series of stairs. The velocities on the stairs obtained from difference are not zero. Correspondingly, it may violate local mass balance. Mei et al. [14, 15] applied different settings for the local mass balance in curved boundary. The velocity on the moving boundary are also not zero in LBM. Coupanec

*Corresponding Author: zhangyu@missouri.edu

and Verschaeve derived a mass conserving boundary condition for tangentially moving walls in LBM [16]. An enhanced mass conserving closure scheme was employed for LBM hydrodynamics for open boundary condition [17]. There are some different opinions about local mass balance. It was argued that this local mass balance is fundamentally flawed which will lead incorrect pressure [18, 19]. Ginzbourg and d'Humieres demonstrated that the total mass balance can be reached even though the local mass balance is not satisfied in LBM boundary condition [20]. Mass and momentum transfer across the curved boundary in LBM are reviewed in Ref. [11]. They concluded that including momentum addition to density distribution reduction had no direct influence on flow and pressure fields, but the incorrect fluid-particle interaction might affect simulation results of particulate suspensions. Mass balance is conservation law based on macroscopic parameters velocity and density, and local mass balance has no direct relation with conservation law since it is based on mesoscopic parameter density distribution. In this paper, LBM with three common boundary conditions (Zou-He method, finite difference velocity gradient method, and regularized method) are employed to solve the fluid flow problem with velocity Dirichlet boundary. All three methods can not satisfy local mass balance for the non-zero boundary. These three boundary conditions will be discussed based on mass conservation law directly.

2. PROBLEM STATEMENT

Poiseuille flow is employed to test the boundary methods in LBM for velocity Dirichlet condition. Figure 1 shows 2-D incompressible fluid flow between two parallel flat plates. The channel's height and length are h and l, respectively. Fully-developed flow can be reached at the channel outlet since l is greater than $10h$.

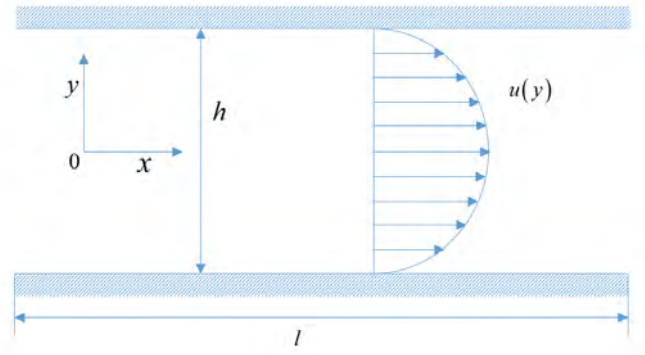

Fig. 1 Physical model

This problem is governed by the following equations

$$\frac{\partial \rho}{\partial t}+\frac{\partial(\rho u)}{\partial x}+\frac{\partial(\rho v)}{\partial y}=0 \tag{1}$$

$$\frac{\partial(\rho u)}{\partial t}+\frac{\partial(\rho u u)}{\partial x}+\frac{\partial(\rho v u)}{\partial y}=-\frac{\partial p}{\partial x}+\mu\left(\frac{\partial^2 u}{\partial x^2}+\frac{\partial^2 u}{\partial y^2}\right) \tag{2}$$

$$\frac{\partial(\rho v)}{\partial t}+\frac{\partial(\rho u v)}{\partial x}+\frac{\partial(\rho v v)}{\partial y}=-\frac{\partial p}{\partial y}+\mu\left(\frac{\partial^2 v}{\partial x^2}+\frac{\partial^2 v}{\partial y^2}\right) \tag{3}$$

which are subject to the following boundary conditions:

$$x=0:\ u=u(y)\ \ v=0 \tag{4}$$

$$x=l:\ \partial u/\partial x=0\ \ v=0 \tag{5}$$

$$y=h/2:\ u=0\ \ v=0 \tag{6}$$

$$y=-h/2:\ u=0\ \ v=0 \tag{7}$$

In addition, the Reynolds number is defined using maximum velocity $u_{\max}$ in the channel.

$$\mathrm{Re} = \frac{u_{\max} h}{\nu} \tag{8}$$

3. LATTICE BOLTZMANN METHOD

Statistical behavior of fluid flow can be expressed by the following Boltzmann equation [4].

$$\frac{\partial f}{\partial t} + \boldsymbol{\varepsilon} \cdot \frac{\partial f}{\partial \boldsymbol{r}} + \boldsymbol{a} \cdot \frac{\partial f}{\partial \boldsymbol{\varepsilon}} = \Omega(f)_{collision} \tag{9}$$

where f and Ω are density distribution and collision operator, respectively. Lattice Boltzmann method is executed on a regular grid. For a 2-D problem, density distributions on each computing node have nine directions to move to the nearby nodes, which is shown in Fig. 2. This is referred to as D2Q9 model in LBM [21].

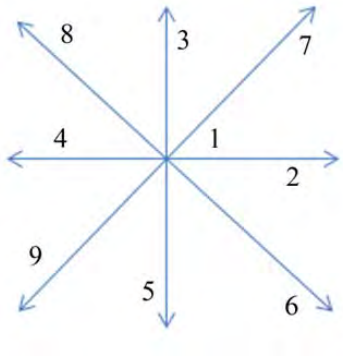

Fig. 2 Nine directions in D2Q9 model

The velocities on each node are:

$$e_a = \begin{cases} (0,0) & a = 1 \\ c(-\cos\frac{a\pi}{2}, -\sin\frac{a\pi}{2}) & a = 2,3,4,5 \\ \sqrt{2}c(-\cos\frac{(2a+1)\pi}{4}, -\sin\frac{(2a+1)\pi}{4}) & a = 6,7,8,9 \end{cases} \tag{10}$$

where c is the lattice speed. Then Eq. (9) can be differenced in these nine directions as follows:

$$f_a(x + e_a \Delta t, t + \Delta t) - f_a(x,t) = \Omega_a(f)_{collision} \qquad a = 1,2,\cdots,9 \tag{11}$$

where Δt is discrete time step. One LBM iteration includes two steps: collision and streaming. The collision step is local to each node.

$$f_a^*(x,t) = f_a(x,t) + \Omega_a(f)_{collision} \qquad a = 1,2,\cdots,9 \tag{12}$$

where f^* is the post-collision density distribution. Many methods exist in LBM to simplify the collision term. The algorithms can be single relaxation time model (SRT), double relaxation time model, or multiple relaxation time model. Double relaxation and multiple relaxation time models have better numerical stability than SRT. On the other hand, SRT has valid advantages in simple model setting. SRT is employed since numerical stability isn't challenging for all the test cases in this article. This model simplifies the collision operator by the following equation:

$$\Omega_a(f)_{collision} = -\frac{1}{\tau}\left(f_a - f_a^{eq}\right) \qquad a = 1,2,\cdots,9 \tag{13}$$

where τ is the single relaxation time, and f_a^{eq} is the direction equilibrium distribution

$$f_a^{eq} = \rho\omega_a\left(1 + \frac{1}{c_s^2}\boldsymbol{e_a}\cdot\boldsymbol{V} + \frac{1}{2c_s^4}\boldsymbol{Q_a}:\boldsymbol{VV}\right) \qquad a = 1,2,\cdots,9 \tag{14}$$

where c_s is the speed of sound which equals $c/\sqrt{3}$. The scalar lattice weights ω_a and tensors $\boldsymbol{Q_a}$ are defined as:

$$\omega_a = \begin{cases} \frac{4}{9} & a = 1 \\ \frac{1}{9} & a = 2,3,4,5 \\ \frac{1}{36} & a = 6,7,8,9 \end{cases} \tag{15}$$

$$\boldsymbol{Q_a} = \boldsymbol{e_a}\boldsymbol{e_a} - c_s^2\boldsymbol{I} \qquad a = 1,2,\cdots,9 \tag{16}$$

where $\boldsymbol{I}$ is the unit tensor. The local collision step can be fulfilled by the settings above. Streaming step follows the collision step and it takes the post-collision distributions to the nearby nodes.

$$f_a(x + e_a\Delta t, t + \Delta t) = f_a^*(x,t) \qquad a = 1,2,\cdots,9 \tag{17}$$

The macroscopic variables can be obtained by moments of the density distributions. ρ, $\rho\boldsymbol{V}$ and $\prod$ correspond to density distribution momentums of 0, 1 and 2.

$$\rho = \sum_{a=1}^{9} f_a \tag{18}$$

$$\rho\boldsymbol{V} = \sum_{a=1}^{9} \boldsymbol{e_a} f_a \tag{19}$$

$$\prod = \sum_{a=1}^{9} \boldsymbol{Q_a} f_a \tag{20}$$

$$p = \rho c_s^2 \tag{21}$$

Applying the following Chapman-Enskog expansion equations

$$\frac{\partial}{\partial r} = K\frac{\partial}{\partial r_1} \tag{22}$$

$$\frac{\partial}{\partial t} = K\frac{\partial}{\partial t_1} + K^2\frac{\partial}{\partial t_2} \tag{23}$$

$$f_a = f_a^0 + Kf_a^1 + K^2 f_a^2 \tag{24}$$

to Eq. (11), the macroscopic governing equations can be obtained from LBM:

$$\frac{\partial \rho}{\partial t} + \nabla\cdot(\rho \boldsymbol{V}) = 0 \tag{25}$$

$$\frac{\partial(\rho \boldsymbol{V})}{\partial t} + \nabla\cdot(\rho \boldsymbol{V}\boldsymbol{V}) = -\nabla p + \nabla\cdot\left[\rho\Delta t\left(\tau - \frac{1}{2}\right)c_s^2\left(\nabla \boldsymbol{V} + (\nabla \boldsymbol{V})^T - \frac{1}{c_s^2}\nabla\cdot(\rho \boldsymbol{V}\boldsymbol{V}\boldsymbol{V})\right)\right] \tag{26}$$

To reach the Navier-Stokes equations, the relaxation time τ is related to ν by:

$$\Delta t\left(\tau - \frac{1}{2}\right)c_s^2 = \nu \tag{27}$$

$K^2 f_a^2$ in Eq. (24) shows no effect in this process. Equation (26) differs from the momentum equation due to presence of the term $\nabla\cdot\left[\rho\left(-\frac{\nu}{c_s^2}\nabla\cdot(\rho \boldsymbol{V}\boldsymbol{V}\boldsymbol{V})\right)\right]$. It can be neglected when Mach number is low that is the case in consideration. In the multiscales analysis process, the following equations are also reached:

$$\begin{cases} f_a^0 = f_a^{eq} \\ Kf_a^1 = -\dfrac{\rho\tau\omega_a}{c_s^2}\boldsymbol{Q_a} : \nabla \boldsymbol{V} \end{cases} \qquad a = 1,2,\cdots,9 \tag{28}$$

Neglecting the high order term effect, density distributions are approximated as:

$$f_a = f_a^{eq} - \frac{\rho\tau\omega_a}{c_s^2}\boldsymbol{Q_a} : \nabla \boldsymbol{V} \qquad a = 1,2,\cdots,9 \tag{29}$$

This equation plays important roles in many boundary conditions.

4. IMPLEMENT OF BOUNDARY CONDITIONS

The density distributions in some directions are unknown on the boundary before the collision step. Fig. 3 shows the left boundary in a 2-D domain.

The density distributions f_2, f_6, and f_9, shown by dark vectors, are unknown after the streaming step. The LBM boundary conditions are designed to find these unknown density distributions. Some boundary conditions substitute the unknown density distributions and keep the known ones. In contract, some methods replace all the density distributions on boundaries before the collision step. Boundary conditions also differ from each other by the relation with the other nearby nodes. Some methods obtain the boundary distributions based on the local computation node information only, while others need the nearby nodes information to recover the boundary distributions. This article compares three common methods (Zou-He [22], finite difference velocity gradient [23] and regularized method [24]) for velocity Dirichlet boundary conditions. Table 1 summarize the categories for these three methods. Boundary velocities are known in Dirichlet condition. Three

boundary conditions in consideration are described for velocity Dirichlet condition based on left boundary in Fig. 3.

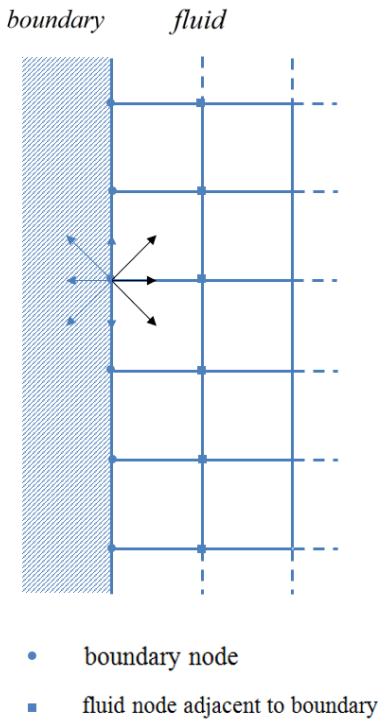

Fig. 3 Boundary and fluid nodes

4.1 Zou-he boundary (BC1)

This method recoveries the missing density distributions based on the local information only [22]. In this 2-D problem, Eqs. (18) and (19) are:

$$\begin{cases} f_1 + f_2 + f_3 + f_4 + f_5 + f_6 + f_7 + f_8 + f_9 = \rho \\ f_2 + f_6 + f_9 - f_4 - f_7 - f_8 = \rho u \\ f_3 + f_6 + f_7 - f_5 - f_8 - f_9 = \rho v \end{cases} \tag{30}$$

where u and v are known in velocity Dirichlet condition. Four independent unknowns (ρ, f_2, f_6 and f_9) in three equations indicates one degree of freedom is left. Meanwhile, density distribution can be obtained directly from Eq. (30).

$$\rho = \frac{f_1 + f_3 + f_5 + 2\times(f_4 + f_7 + f_8)}{1+u} \tag{31}$$

In Zou-He boundary condition, the nonequilibrium parts are assumed to be the same in directions 2 and 4.

$$f_2 = f_2^{eq} + f_4 - f_4^{eq} \tag{32}$$

and $\frac{\tau\omega_2}{c_s^2}\boldsymbol{Q}_2:\rho\nabla\boldsymbol{V}$ equals to $\frac{\tau\omega_4}{c_s^2}\boldsymbol{Q}_4:\rho\nabla\boldsymbol{V}$ due to the symmetry of $\boldsymbol{Q}$. Therefore this assumption is reasonable regarding the Eq. (27). Then the other two missing density distributions are:

$$\begin{cases} f_6 = (f_4 + f_5 + 2\times f_8 - f_2 - f_3 + \rho u + \rho v)/2 \\ f_9 = (f_3 + f_4 + 2\times f_7 - f_2 - f_5 + \rho u - \rho v)/2 \end{cases} \tag{33}$$

4.2 Finite difference velocity gradient method (BC2)

This method is based on the approximation in Eq. (29) with slight difference [23].

$$f_a = f_a^{eq} - \frac{\tau\omega_a}{c_s^2}\boldsymbol{Q}_a:\nabla(\rho\boldsymbol{V}) \qquad a = 1,2,\cdots,9 \tag{34}$$

Different from Eq. (29), ρ is inside the operator ∇. This setting includes the compressible effect in the strain rate, which is negligible for the incompressible fluid flow in this article. Boundary density is obtained from Eq. (30) and then $\nabla(\rho\boldsymbol{V})$ is obtained by the following equation:

$$\nabla\boldsymbol{V} = \begin{bmatrix} \partial(\rho u)/\partial x, \partial(\rho v)/\partial x \\ \partial(\rho u)/\partial y, \partial(\rho v)/\partial y \end{bmatrix} \tag{35}$$

Three computing nodes in one direction are shown in Fig. 4.

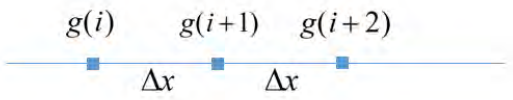

Fig. 4 Difference model

To maintain the second order accuracy, three point midpoint and endpoint derivative laws are employed for the operators in Eq. (35).

$$\begin{cases} g'(i) = \frac{1}{2\Delta x}\left[-3\times g(i) + 4\times g(i+1) - g(i+2)\right] \\ g'(i+1) = \frac{1}{2\Delta x}\left[-g(i) + g(i+2)\right] \\ g'(i+2) = \frac{1}{2\Delta x}\left[g(i) - 4\times g(i+1) + 3\times g(i+2)\right] \end{cases} \tag{36}$$

Then all the boundary density distributions can be obtained from by Eq. (34)

4.3 Regularized method (BC3)

Similar to finite velocity gradient method, the regularized method [24] also replaces all the boundary density distributions with Eq. (29). Instead of calculating $\nabla\boldsymbol{V}$ from the nearby nodes information, regularized method fulfills this step using the local information. The strain rate tensor S is defined as $\frac{1}{2}\left[\nabla\boldsymbol{V} + (\nabla\boldsymbol{V})^T\right]$. Due to the symmetry of $\boldsymbol{Q}_a$ and S, Eq. (29) becomes the following equation:

$$f_a = f_a^{eq} + \frac{\omega_a}{2c_s^4} Q_a : \Pi^{(1)} \qquad a = 1, 2, \cdots, 9 \tag{37}$$

where the tensor $\Pi^{(1)}$ is defined as:

$$\Pi^{(1)} = -2c_s^2 \tau \rho \boldsymbol{S} \tag{38}$$

After boundary density ρ is solved from the Eq. (30), f_a^{eq} can be obtained by Eq. (14). $\Pi^{(1)}$ is approximated by the following equation:

$$\Pi^{(1)} = \Pi^{(neq)} = \sum_{a=1}^{9} \boldsymbol{Q}_a f_a^{neq} \tag{39}$$

Not all f_a^{neq} are known after the streaming process. For example, f_2^{neq}, f_6^{neq} and f_9^{neq} are unknowns for the left boundary. They are approximated to equal that in the opposite directions.

$$f_2^{neq} = f_4^{neq},\ f_6^{neq} = f_8^{neq},\ f_9^{neq} = f_7^{neq} \tag{40}$$

Then regularized method if fulfilled by the equations above.

5. RESULTS AND DISCUSSIONS

To test the three methods for velocity Dirichlet boundary conditions, Poiseuille flows in Section 2 are solved with LBM using them respectively. *Re* in test cases are 5, 10, 25, 50 to limit the compressible effects. After grid size independent test, 30×500 grids are employed for all the test cases.

Analytical solution exists in this problem once fully development is reached [10].

$$u(y) = u_{\max}\left[1 - \left(\frac{2y}{h}\right)^2\right] \tag{41}$$

where $u_{\max}$ is the maximum velocity. Then u is quadratic to the location y. p_x. p_x is the average pressure along y. It is linear to x according to the analytical solution. Assuming Δp to be the pressure difference between p_x and p_{out}, then Δp is also linear to x.
Each case has same τ in Eq. (27) by adapting u_0. LBM simulation is carried on till steady-state condition is reached.

$$\max\left|\frac{u_t - u_{t-1}}{u_t}\right| \le 10^{-10} \tag{42}$$

Then numerical solutions are compared with analytical results for validation.

Figure 5 shows the comparison of velocities between LBM and analytical results for Re = 5. These two quadratic results agree with each other well. Figure 6 shows the comparison of pressure differences. They are all linear to x and agree with each other well. Therefore, numerical results with different boundary conditions agree with the analytical results well in this case.

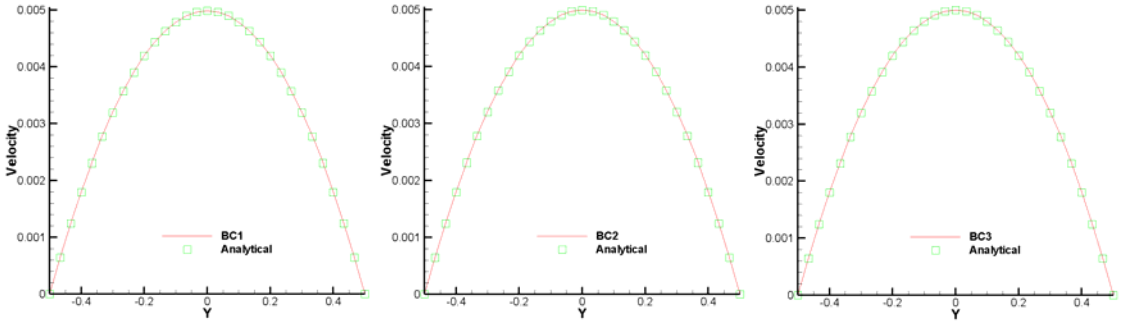

(a) BC1 (b) BC2 (c) BC3

Fig. 5 Velocity distribution, Re=5

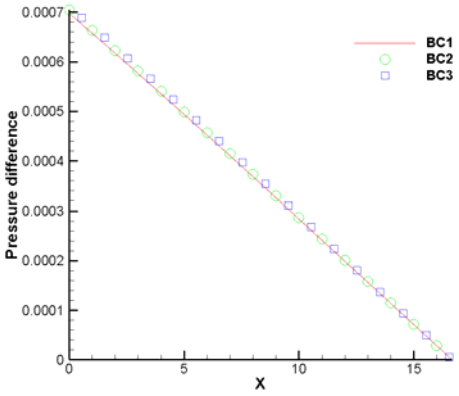

Fig. 6 Pressure distribution, Re=5

Figures 7 and 8 show the velocity and pressure comparisons for Re = 10. Velocities are still quadratic to y and agree with the analytical results well. The maximum velocity u_{max} increases to 0.01 from 0.005 as Re increases from 5 to 10. All three boundary conditions also lead to the same Δp results which are linear to x. The slop is also twice as that for the case of Re =5. Therefore LBM with different boundary conditions can all lead to the results agreeing analytical results well.

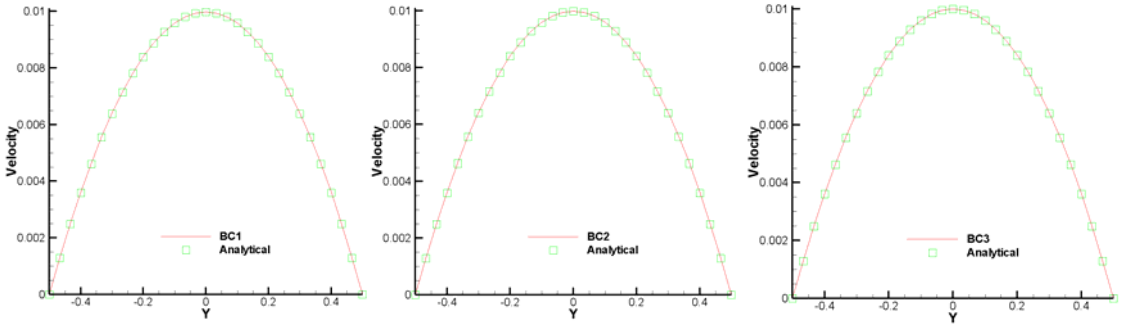

(a) BC1 (b) BC2 (c) BC3

Fig. 7 Velocity distribution, Re=10

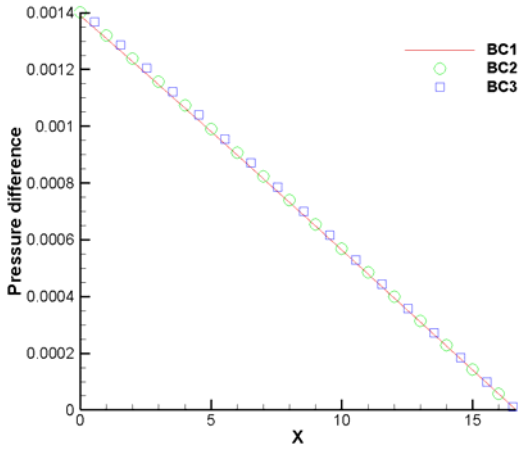

Fig. 8 Pressure distribution, Re=10

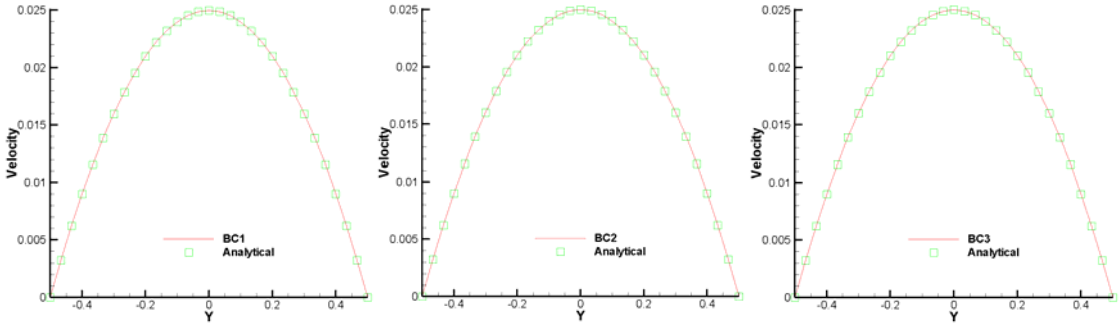

(a) BC1 (b) BC2 (c) BC3

Fig. 9 Velocity distribution, Re=25

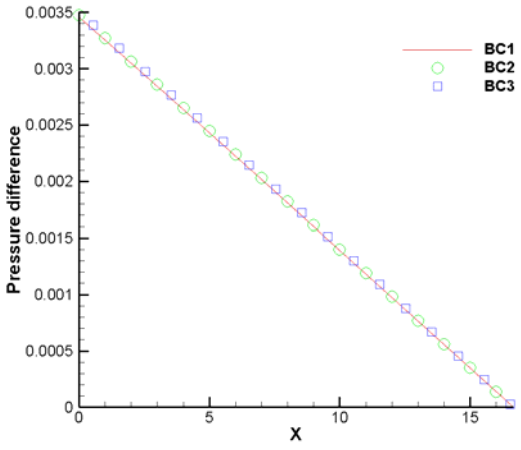

Fig. 10 Pressure distribution, Re=25

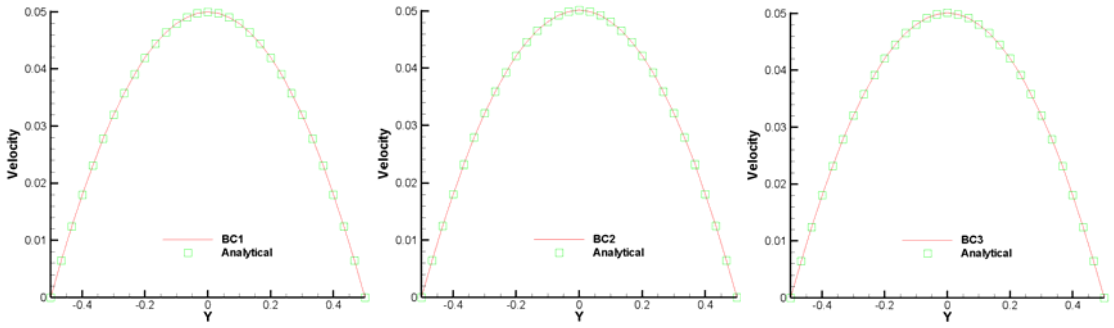

(a) BC1 (b) BC2 (c) BC3

Fig. 11 Velocity distribution, Re=50

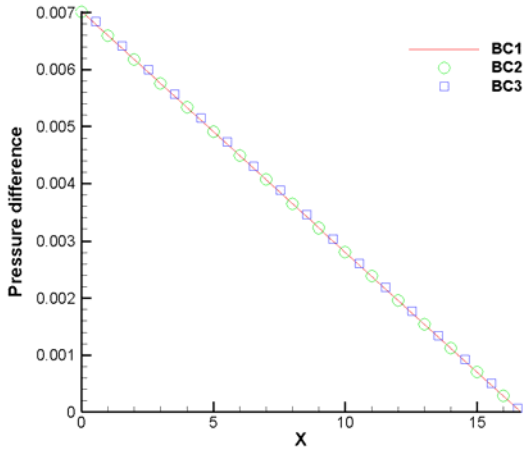

Fig. 12 Pressure distribution, Re=50

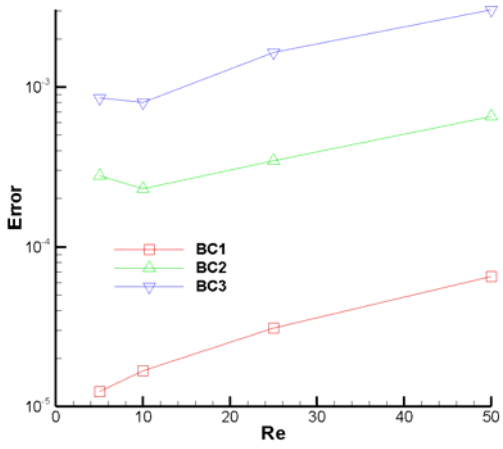

Fig. 13 Error comparison

The test cases are also carried on for Reynolds numbers are 25 and 50. Figures 9-12 are comparisons of velocity and pressure for these two cases. Their analytical results are also satisfied. Therefore LBM with different boundary conditions can lead to results agreeing with analytical results for all the test cases.

It is necessary to point out that these three boundary conditions all violate local mass balance, which does not relate to mass balance directly. The following parameter *MB* is employed to value different boundary conditions' accuracies.

$$MB = max\left|\frac{\partial \rho}{\partial t} + \frac{\partial (\rho u)}{\partial x} + \frac{\partial (\rho v)}{\partial y}\right| \tag{43}$$

This common convergence criterion in CFD is not used widely in LBM. This parameter grows with character velocity growing. To eliminate this effect, we use another error parameter.

$$error = MB / u_{\max} \tag{44}$$

The error tendency with Re for different boundary conditions are shown in Fig. 13.

Numerical methods fit mass balance better with this error decreasing. It changes from 10^{-5} to 10^{-4} for BC1. On the hand, BC2 and BC3 have the errors around 10^{-3}. The BC1 error is less than the other boundary conditions' results by 10 times at least. BC1 results are much better than the other cases from the mass balance point of view.

5. CONCLUSIONS

Three boundary conditions (Zou-He method, finite difference velocity gradient method and regularized method) are tested and compared for velocity Dirichlet condition. Poiseuille flows with different Reynolds numbers are solved for validation. LBM with different boundary conditions velocity and pressure results agree with the analytical solutions well for all the test cases. Meanwhile, LBM with Zou-He boundary condition leads to the results fitting mass balance the best. Therefore, local mass balance has no relation with the macroscopic mass balance in LBM boundary. Zou-He boundary condition is superior in LBM for this kind of problems regarding macroscopic mass balance.

ACKNOWLEDGMENT

Support for this work by the U.S. National Science Foundation under grant number CBET- 1404482, Chinese National Natural Science Foundations under Grants 51129602 and 51276118 are gratefully acknowledged.

NOMENCLATURE

$\boldsymbol{a}$	lattice acceleration	(-)	t	lattice time	(-)
c	lattice speed	(-)	u	horizontal velocity in lattice unit	(-)
c_s	lattice sound speed	(-)	v	vertical velocity in lattice unit	(-)
e_a	velocity in every direction	(-)	U	non-dimensional horizontal velocity	(-)
f	density distribution	(-)	V	non-dimensional vertical velocity	(-)
$\boldsymbol{I}$	unit tensor	(-)	$\boldsymbol{V}$	velocity	(-)
K	Chapman-Enskog expansion coefficient	(-)	$\prod$	stress tensor	(-)
P	non-dimensional pressure	(-)	τ	relaxation time	(-)
$\boldsymbol{Q}$	lattice weight tensor	(-)	ω	lattice weight	(-)
$\boldsymbol{r}$	lattice location vector	(-)	Ω	collision operator	(-)

REFERENCES

[1] Succi S., "Lattice Boltzmann Method for Fluid Dynamics and Beyond", Oxford University Press, (2001).
[2] Zou Q., Hou S., Chen S. and Doolen G., "An improved incompressible lattice Boltzmann model for time-independent flows", Journal of Statistical Physics, 81, pp. 35-48, (1995).
[3] Li Z., Yang M. and Zhang Y., "Hybrid lattice Boltzmann and finite volume methods for fluid flow problems", Journal for Multiscale Computational Engineering, 12(3), pp. 177-192, (2014).
[4] Chen S. and Doolen G., "Lattice Boltzmann method for fluid flows, Annual Review of Fluid Mechanics", 30, pp. 329–364, (1998).
[5] Guo Z. and Zhao T., "Lattice Boltzmann model for incompressible flows through porous media", Physical Review E, 66, pp.

036304, (2002).
[6] Chatterjee D. and Chakraborty S., “An enthalpy-based lattice Boltzmann model for diffusion dominated solid-liquid phase transformation”, Physics Letters A, 341, pp. 320-330, (2005).
[7] Li Z., Yang M. and Zhang Y., “A hybrid lattice Boltzmann and finite volume method for melting with convection, Numerical Heat transfer”, Part B: Fundamentals: An International Journal of Computation and Methodology, 66, pp.307-325, (2014).
[8] Li Z., Yang M. and Zhang Y., “A coupled lattice Boltzmann and finite volume method for natural convection simulation”, International Journal of Heat and Mass Transfer, 70, pp. 864-874, (2014).
[9] Li Z., Yang M. and Zhang Y., “Hybrid lattice Boltzmann and finite volume method for natural convection”, Journal of Thermophysics and Heat Transfer, 28(1), pp. 68-77, (2014).
[10] Latt J. and Chopard B., “Straight velocity boundaries in the lattice Boltzmann method. Physical Review E” 77, pp. 056703, (2008).
[11] Yin X., Le G. and Zhang J., “Mass and momentum transfer across solid-fluid boundaries in the lattice-Boltzmann method”, Physical Review E, 86, pp. 026701, (2012).
[12] Mei R., Luo L., and Shyy W., “An accurate boundary treatment in the lattice Boltzmann method”, Journal of Computational Physics, 155(2), pp. 307-330, (1999).
[13] Mei R., Yu D., Shyy W. and Luo L., “Force evaluation in the lattice Boltzmann method involving curved geometry”, Physical Review E, 65, pp. 041203, (2002).
[14] Bao J., Yuan P. and Schaefer L., “A mass conserving boundary condition for the lattice Boltzmann equation method”, Journal of Computational Physics, 22, pp. 8472-8487, (2008).
[15] Verschaeve J. and Muller B., “A curved no-slip boundary condition for the lattice Boltzmann method”, Journal of Computational Physics, 299, pp. 6781-6803, (2010).
[16] Coupanec E. and Verschaeve J., “A mass conserving boundary condition for the lattice Boltzmann method for tangentially moving walls”, Mathematics and Computers in Simulation 81, pp. 2632-2645, (2011).
[17] Hollis A., Halliday I. and Care C., “Enhanced, mass-conserving closure scheme for lattice Boltzmann equation hydrodynamics”, Journal of Physics A: Mathematical and General, 39, pp. 10589-10601, (2006).
[18] Ladd A. and Verberg R., “Lattice-Boltzmann simulations of particle-fluid suspension”, Journal of Statistical Physics, 104, pp. 1191-1251, (2001).
[19] Nguyen N. and Ladd A., “Lubrication corrections for lattice-Boltzmann simulations of particle suspensions”, Physical Review E, 66, pp. 046708, (2002).
[20] Ginzbourg I. and d’Humieres D., “Local second-order boundary methods for lattice Boltzmann models”, Journal of Statistical Physics, 84(5-6), pp. 927-971, (1996).
[21] Filippova O. and Hanel D., “Grid refinement for lattice-BGK models”, Journal of Computational Physics, 147(1), pp. 219-228, (1998).
[22] Zou Q. and He X., “On pressure and velocity boundary conditions for the lattice Boltzmann BGK model”, Physics of Fluids, 9(6), pp. 1591-1598, (1997).
[23] Skordos P., Initial boundary conditions for lattice Boltzmann method, Physical RevIew E, 48, pp. 4823, (1993).
[24] Latt J., Hydrodynamic Limit of Lattice Boltzmann Equations, PhD Thesis. University of Geneva, (2007).